Satellite Analysis of Tropical Cyclones Using the Advanced Microwave Sounding Unit (AMSU)

Stanley Q. Kidder,* Mitchell D. Goldberg,+ Raymond M. Zehr,#
Mark DeMaria,# James F. W. Purdom,+ Christopher S. Velden,@
Norman C. Grody,& and Sheldon J. Kusselson**

ABSTRACT

The first Advanced Microwave Sounding Unit (AMSU) was launched aboard the *NOAA-15* satellite on 13 May 1998. The AMSU is well suited for the observation of tropical cyclones because its measurements are not significantly affected by the ice clouds that cover tropical storms. In this paper, the following are presented: 1) upper-tropospheric thermal anomalies in tropical cyclones retrieved from AMSU data, 2) the correlation of maximum temperature anomalies with maximum wind speed and central pressure, 3) winds calculated from the temperature anomaly field, 4) comparison of AMSU data with GOES and AVHRR imagery, and 5) tropical cyclone rainfall potential. The AMSU data appear to offer substantial opportunities for improvement in tropical cyclone analysis and forecasting.

1. Introduction

Scientific progress often comes about as a result of new instruments for making scientific observations. The Advanced Microwave Sounding Unit (AMSU) is one such new instrument. The first AMSU was flown on the *NOAA-15* satellite on 13 May 1998, and it will fly on the *NOAA-16* and *NOAA-17* satellites as well. The measuring capabilities of the instrument are detailed in section 3.

One of the most exciting capabilities of the AMSU is the observation of tropical cyclones. The four major reasons for this excitement are the following.

1) The main tropical cyclone parameters of interest to the forecaster are storm location and movement, thermal anomalies, wind speeds, and rain rate. While other satellite instruments can be used to estimate these parameters, the AMSU is the first satellite instrument that has the potential to measure all of them.
2) Since clouds are nearly (but not completely) transparent to microwave radiation, the AMSU can measure the above parameters even through the central dense overcast that prevents visible and infrared satellite instruments from making these measurements.
3) The AMSU has significantly improved spatial resolution, radiometric accuracy, and the number of channels over the previous Microwave Sounding Unit (MSU; see section 3) that has been used for tropical cyclone analysis.
4) The AMSU complements the much more frequent and higher-resolution observations of the geostationary satellites to give a more complete description of tropical storms.

The purpose of this paper is to describe tropical cyclone analysis using AMSU data and to indicate how the data will be useful in forecasting these storms. Section 2 gives a background on satellite observation

*CIRA/Colorado State University, Fort Collins, Colorado.
+NOAA/NESDIS/ORA, Washington, D.C.
#NOAA/NESDIS/RAMM Team, Fort Collins, Colorado.
@CIMSS/University of Wisconsin—Madison, Madison, Wisconsin.
&NOAA/NESDIS/Microwave Sensing Group, Washington, D.C.
**NOAA/NESDIS/SAB, Washington, D.C.
Corresponding author address: Dr. Stanley Q. Kidder, Cooperative Institute for Research in the Atmosphere, Colorado State University, Foothills Campus, Fort Collins, CO 80523-1375.
E-mail: kidder@cira.colostate.edu
In final form 13 December 1999.

of tropical cyclones with emphasis on microwave observations; section 3 describes the measuring capabilities of the new AMSU instrument; section 4 contains examples of tropical cyclone measurements; and conclusions are stated in section 5.

2. Background

The first satellite observations of tropical cyclones were made by low earth orbiting weather satellites. Indeed, since these satellites became operational in the mid-1960s, no tropical cyclone anywhere on earth has gone unobserved. With the advent of geostationary satellites, with their frequent imaging capabilities, the focus of tropical cyclone observation shifted away from low earth orbiting satellites (polar orbiting satellites) to the geostationary satellites and became increasingly important (Purdom and Menzel 1996; DeMaria 1996). Dr. R. Sheets (1990), then director of the National Hurricane Center (NHC), stated, "If there were a choice of only one observing tool for meeting the responsibility of the NHC, the author would clearly choose the geostationary satellite."

Using imagery from polar orbiting satellites, Dvorak (1973, 1975) developed a technique, which has undergone refinement but is still in use today, to estimate tropical cyclone intensity. That technique uses information gleaned from a storm's cloud pattern [curvature, spiral banding, eye, central dense overcast (CDO)] and the day-to-day changes in that pattern in visible imagery to assess the stage of development of a tropical storm. Later, the technique was expanded to accommodate characteristics revealed in infrared imagery from geostationary satellites (Dvorak 1984), and it has been automated (Velden et al. 1998). Sheets (1990) pointed to "the development of the Dvorak technique ... [as] the single greatest achievement in support of operational tropical cyclone forecasting by a researcher to date."

In parallel with advances in visible and infrared observations of tropical cyclones were observations in the microwave portion of the electromagnetic spectrum—all made from low earth orbiting satellites. Microwave observations have two main advantages over visible or infrared observations: 1) microwave radiation penetrates clouds, and 2) microwave radiation is sensitive to a wide variety of geophysical parameters, among them atmospheric temperature and moisture, cloud liquid water, cloud ice water, rain, and surface wind speed.

Microwave observations of tropical cyclones have a long history. Rosenkranz et al. (1978) first noticed a warm anomaly in data from the *Nimbus-6* Scanning Microwave Spectrometer over Typhoon June. Kidder et al. (1978) showed that the warm anomaly was the result of upper-level warming over tropical storms that can be detected through the clouds by the microwave sounder. They further showed that the magnitude of the warm anomaly in the microwave data is related to the storm's central pressure and outer winds. Kidder et al. (1980) improved on the latter relationship. Velden and Smith (1983), Velden (1989), and Velden et al. (1991) used brightness temperatures and 250-mb temperatures retrieved from MSU data to estimate the intensity and central pressure of a large sample of tropical cyclones and found good agreement with aircraft and other methods. Grody (1979) introduced the wind weighting function concept to study the winds in Typhoon June using the horizontal gradient of the microwave measurements. Grody and Shen (1982) extended this work using MSU data for Hurricane David. This study employed rawinsonde data to show the exceptionally high correlation (> 0.9) between the MSU brightness temperature gradient and the actual winds around 500 mb. Microwave data have also been used to study precipitation in tropical cyclones. Allison (1974) used *Nimbus-5* Electrically Scanning Microwave Radiometer data to study tropical cyclone rainfall. Many others have continued these studies (e.g., Adler and Rodgers 1977; Rodgers and Adler 1981). Recently Spencer (1993) succeeded in retrieving precipitation measurements from MSU data even though they were designed for sounding, not precipitation measurement. Precipitation measurements in tropical storms by the Tropical Rainfall Measuring Mission (TRMM)—and particularly by its TRMM Microwave Imager (TMI) and Precipitation Radar instruments (Kummerow et al. 1998)—appear especially promising.

Most previous studies of tropical cyclones using microwave data have suffered from the relatively low resolution of microwave observations. The AMSU has much higher resolution (by a factor of ~2) than previous microwave sounding instruments. The questions before us now are the following.

1) Can we use the higher-resolution thermodynamic information from the AMSU—along with surface-based and aircraft observations and geostationary imagery—to improve the estimate of the tropical cyclone's intensity?

TABLE 1. Microwave instrument comparison [after Kidder and Vonder Haar (1995)]. TMI information from Kunnerow et al. (1998).

Parameter	SSM/T	SSM/T-2	SSM/I	TMI	MSU	AMSU-A	AMSU-B
Satellites	DMSP	DMSP	DMSP	TRMM	*NOAA-6–14*	*NOAA-15+*	*NOAA-15+*
Channels	7	5	7	9	4	15	5
Frequency range (GHz)	50.5–59.4	91.6–183.3	19.35–85.5	10.65–85.5	50.3–57.95	23.8–89.0	89.0–183.3
NEΔT (K)	0.4–0.6	0.5	0.4–1.7	0.3–0.9	0.3	0.25–1.20	0.8
Beamwidth	14°	3.3°–6.0°	0.3°–1.2°	0.4°–3.7°	7.5°	3.3°	1.1°
Scan type	Cross track	Cross track	Conical	Conical	Cross track	Cross track	Cross track
Best ground resolution (km)	204	48–84	12.5–50	5–37	110	48	16
Scan steps	7	28	64–128	26–208	11	30	90
Swath width (km)	2053	2053	1394	759	2347	2179	2179

2) Can other important information be extracted on such parameters as eye size, maximum wind, near-surface field structure, and the radius of gale force winds?
3) Can we utilize the moisture information in the AMSU data to calculate rainfall potential?

3. The AMSU instrument and retrieved parameters

The Advanced Microwave Sounding Unit is a considerable advance over previous microwave instruments. As detailed in Table 1, the AMSU has more channels, better spatial resolution, and improved radiometric accuracy than previous sounding instruments. [Imaging instruments, such as the Special Sensor Microwave/Imager (SSM/I) or the related TMI, have higher resolution.] Figure 1 compares the spatial resolution of the AMSU to the MSU, which has flown on the *TIROS-N* and *NOAA-6–14* satellites since 1978.

Figure 2 and Table 2 show that the AMSU combines the characteristics of several previous instruments. It has the temperature sounding capabilities of the Special Sensor Microwave/Temperature (SSM/T) and MSU, the moisture sounding capabilities of the Special Sensor Microwave/Temperature 2 (SSM/T2), and the ability to retrieve geophysical parameters similar to the SSM/I. In short, because microwaves penetrate clouds, the AMSU can be described as a high-resolution, nearly all-weather meteorological instrument. Figure 3

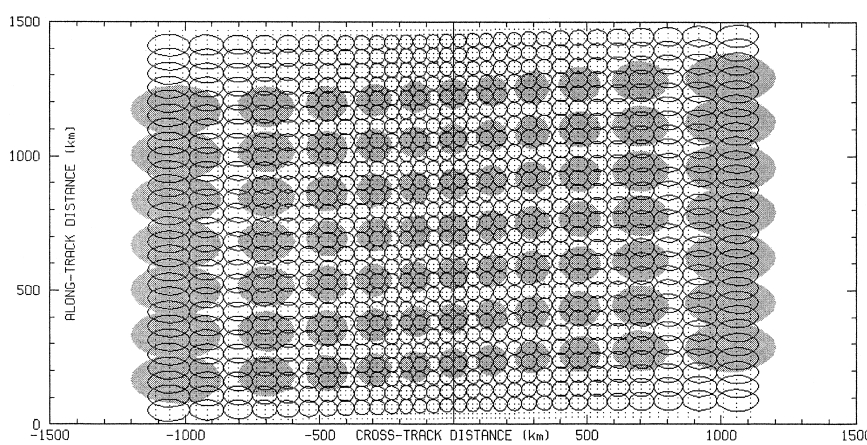

FIG. 1. The filled gray ellipses illustrate the 110-km resolution of the MSU. The black outlined ellipses illustrate the 48-km resolution of the AMSU-A instrument. The black dots mark the centers of the scan spots of the 16-km resolution AMSU-B instrument.

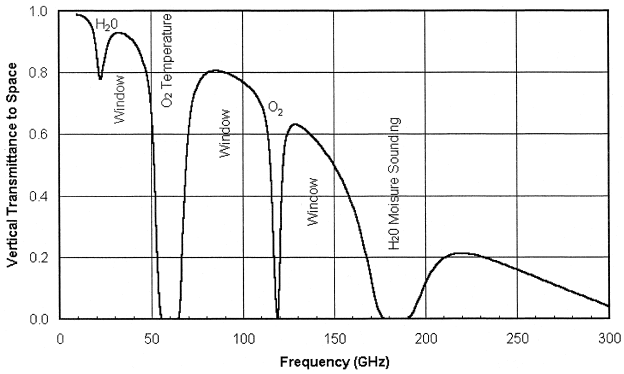

FIG. 2. Microwave spectrum in the 15°N annual atmosphere.

illustrates the dramatic improvement of the AMSU over the MSU for tropical cyclone observation.

The AMSU actually consists of three separate instruments: AMSU-A1, which has AMSU-A channels 3–15; AMSU-A2, which has channels 1 and 2; and AMSU-B, which has five channels usually numbered 16–20. AMSU-A1 and AMSU-A2 are collectively referred to as AMSU-A. Temperature sounding is the chief job of AMSU-A, but several geophysical parameters can be retrieved from it as well, including total precipitable water, cloud liquid water, rain rate, snow cover, and sea ice cover. The chief mission of AMSU-B is to make moisture soundings. In orbit, the AMSU-B instrument has suffered from radio frequency interference from one of the *NOAA-15* downlink antennas. This has caused noise in the signal and has prevented the retrieval of moisture soundings. A correction is under development. In the meantime,

TABLE 2. Microwave frequencies (GHz) (Notation: $x \pm y \pm z$; x is the center frequency. If y appears, the center frequency is not sensed, but two bands, centered at $x \pm y$, are sensed. If z appears, four bands are sensed at frequencies $(x - y) \pm z$ and $(x + y) \pm z$. This scheme increases the signal and, therefore, decreases the noise. V = vertical, H = horizontal, R = rotates with scan angle.) and polarizations. [After Kidder and Vonder Haar (1995). TMI information from Kummerow et al. (1998).]

Channel	SSM/T	SSM/T-2	SSM/I	TMI	MSU	AMSU-A	AMSU-B
1	50.5H	183.3 ± R	19.35H	10.65V	50.30R	23.8R	89.0R
2	53.2H	183.3 ± 1R	19.35V	10.65H	53.74R	31.4R	150.0R
3	54.35H	183.3 ± 7R	22.235V	19.35V	54.96R	50.3R	183.3 ± 1R
4	54.9H	91.7R	37.0H	19.35H	57.95R	52.8R	183.3 ± 3R
5	58.4V	150R	37.0V	21.3V		53.6R	183.3 ± 7R
6	58.825V		85.5H	37.0V		54.4R	
7	59.4V		85.5V	37.0H		54.9R	
8			85.5V			55.5R	
9			85.5H			57.2R	
10						57.29 ± 0.217R	
11						57.29 ± 0.322 ± 0.048R	
12						57.29 ± 0.322 ± 0.022R	
13						57.29 ± 0.322 ± 0.010R	
14						57.29 ± 0.322 ± 0.0045R	
15						89.0R	

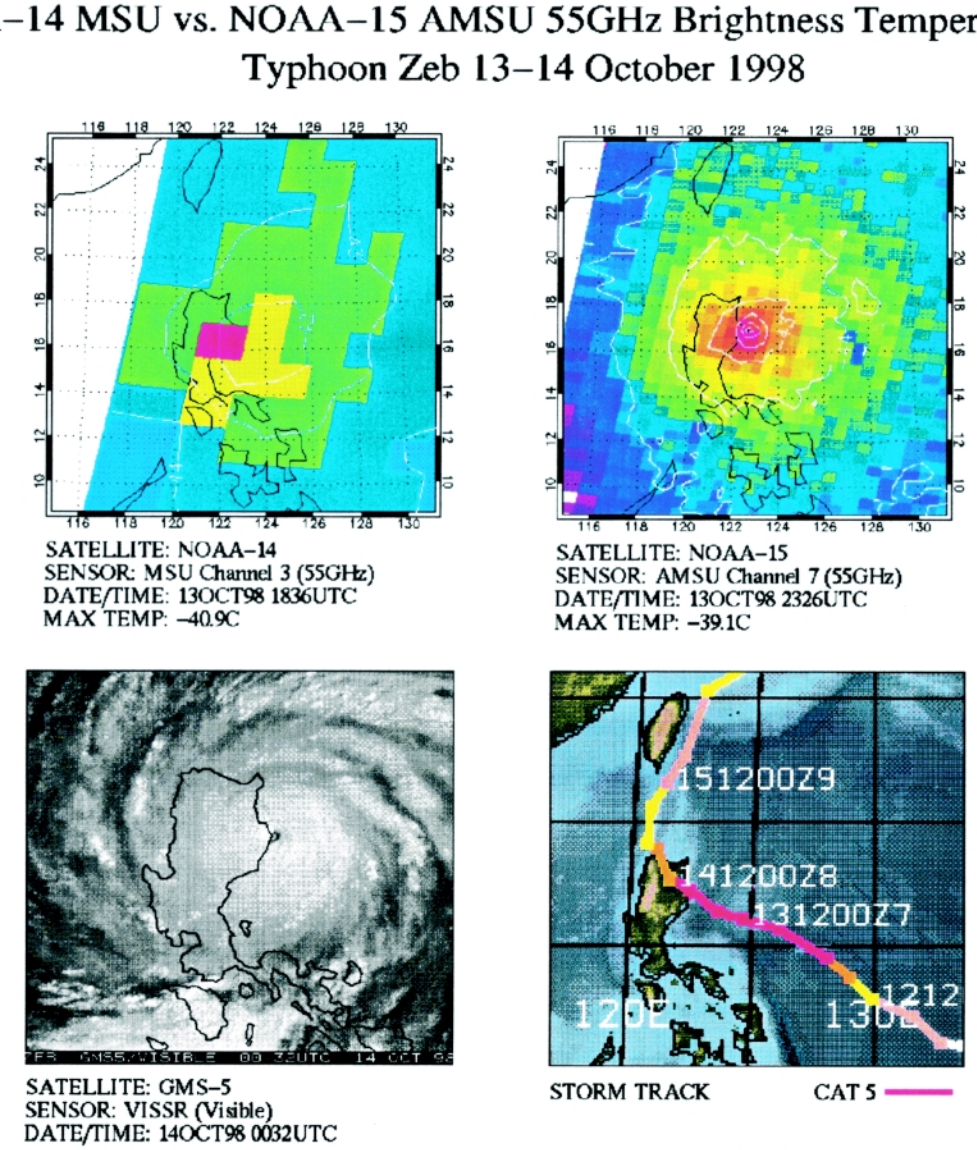

FIG. 3. An illustration of the improvement in spatial resolution of the AMSU over the MSU for Typhoon Zeb.

the AMSU-B imagery is useful for locating clouds and storms.

a. Temperature profile retrieval

Retrieval of atmospheric temperatures from AMSU data has several steps, but is straightforward. Before the temperature retrieval itself can be accomplished, two corrections to the data are made.

The first correction is for antenna sidelobes. At each scan position, the main antenna lobe points at the earth, but sidelobes can point at different points on the earth, at cold space, and at the spacecraft itself. The raw measurements, called antenna temperatures, are converted to brightness temperatures using an algorithm by Mo (1999) that is designed to remove the sidelobe contributions based on model calculations using the AMSU antenna pattern, its scan pattern, and the spacecraft geometry.

The second and larger correction adjusts the brightness temperatures from the 30 different view angles to appear to be nadir observations. This step is called limb adjustment and is based on Wark (1993). As the instrument scans away from nadir, the atmospheric levels (or vertical region) being sensed by a particular channel rise due to the increased pathlength through the upper levels of the atmosphere. If there were no limb adjustment, the brightness temperature for an atmospheric channel could vary by almost 15 K

along a scan line due to vertical variation of atmospheric temperature. Limb adjustment removes this effect. Thirty-one days (1–31 July 1998) of data were used to compute mean brightness temperatures within 2° latitude bands for each scan position. A large sample was used to ensure that differences in mean brightness temperature between two given scan positions are due to view angle and not due to atmospheric variability. Regression coefficients were then computed to adjust measurements from a given scan position to the average of beam positions 15 and 16 (there is no true nadir observation). A global set of coefficients is used for channels 6–14. Sea and nonsea coefficients are used for channels affected by the surface—channels 1–5 and 15.

Atmospheric temperature is retrieved from the limb-adjusted brightness temperatures using regression analysis. The regression coefficients to estimate temperature between the surface and 10 mb from AMSU observations were generated from collocated AMSU-A limb-adjusted brightness temperatures and radiosonde temperature profiles. Normalizing all the observations to nadir results in a large ensemble of collocated radiosonde and AMSU-A data, which is important for deriving a globally representative and stable regression solution. If the data were not limb adjusted, regression coefficients would need to be generated for each scan angle, which could result in scan-angle-dependent biases in the retrieval product due to varying sample size at different scan angles.

The collocated data used in generating the retrieval coefficients were from July and August 1998. Above 10 mb, the lack of radiosonde reports required the regression coefficients to be generated from brightness temperatures simulated from a set of rocketsonde profiles. Different channel combinations are used for different atmospheric levels. For example, channels 1–7 are not used for retrievals above 100 mb to ensure that there is no contamination from high terrain or from contamination by intense precipitation. Similarly, channels 1–5 are not used for retrievals from 700 to 115 mb in order to reduce the contamination from precipitation. A global set of coefficients is used from 700 mb and above, whereas separate coefficients for sea and nonsea are used from 780 to 1000 mb. At present no corrections are made for precipitation effects when using channels 4–6 to retrieve temperatures below 700 mb. The weighting functions of the AMSU channels used in the retrieval algorithm are shown in Fig. 4. The root-mean-square (rms) differences between AMSU-A temperature retrievals and collocated radiosondes for the latitude range of 0°–30°N and the period 1 September to 30 November 1998 are shown in Fig. 5. The rms errors are below 2°C, which is sufficiently low to monitor the thermal structure within tropical cyclones. Additional details on the limb adjustment and temperature retrieval procedures and accuracies are given in Goldberg (1999).

b. Geophysical parameter retrieval

The AMSU was designed primarily to improve the accuracy of temperature soundings beyond that of the four-channel MSU. To achieve this improvement, the AMSU-A module includes 12 channels in the 50–60-GHz portion of the oxygen band to provide temperature soundings from the surface to about 1 mb. AMSU-A also has window channels at 31.4 and 89 GHz to monitor surface features and precipitation and a 23.8-GHz channel for obtaining the total precipitable water over oceans (Grody et al. 1999). Five channels are included in the AMSU-B module: 89- and 150-GHz window channels and three channels around the 183.31-GHz water vapor line for deriving moisture profiles at low to midlevels. All AMSU-A channels have 48-km resolution at nadir; all AMSU-B channels have 16-km resolution at nadir.

In addition to the temperature information, the estimates of precipitation, cloud liquid water, and water

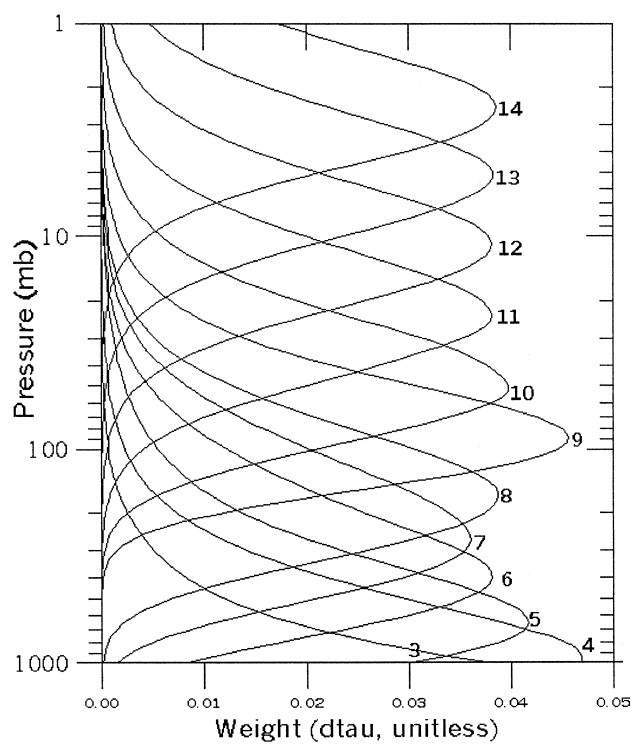

FIG. 4. AMSU weighting functions.

vapor are of importance for monitoring the development of tropical cyclones (and for detecting rain contamination of temperature soundings). The algorithms for deriving these quantities are similar to those developed for the SSM/I (Weng and Grody 1994); the major difference is the need to correct for scan angle (i.e., limb) effects. Dual-frequency measurements (i.e., 23.8 and 31.4 GHz) are used to derive the water vapor and cloud liquid water. Precipitation is identified when the liquid water exceeds a threshold value of about 0.3 mm, while lower values are considered rain free. This technique of measuring precipitation is referred to as the emission approach since it uses low-frequency emission measurements over oceans. A different technique uses the high-frequency scattering by millimeter-size ice particles to estimate rain rates. It was originally developed by the SSM/I and SSM/T2 and is appealing since it is applicable over land as well as oceans (Grody 1991). Also, since the scattering technique uses the highest-frequency channels (e.g., 89 and 150 GHz), the precipitation can be observed at the highest resolution, which is 16 km at nadir using the AMSU-B module (AMSU-A also has an 89-GHz channel, but with a resolution of 48 km.)

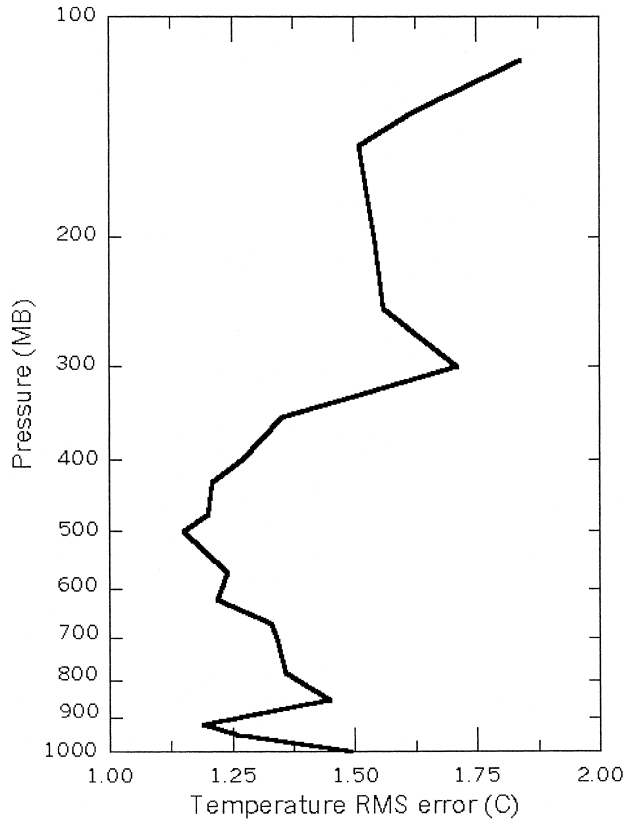

FIG. 5. Rms errors in AMSU temperature retrievals.

4. Applications to tropical cyclone analysis

Traditionally, data from polar orbiting satellites have been used in the initialization of numerical weather prediction models but not by forecasters (except in the high latitudes and by the military). Forecasters usually prefer geostationary data because of the frequent imaging capability. Although microwave data are not yet available from geostationary satellites, they offer capabilities that are useful to both tropical cyclone researchers and forecasters. We present five research and forecasting capabilities made possible by the AMSU.

a. Upper-tropospheric temperature anomalies

The AMSU can sense through the cloud-covered areas of severe storms and tropical cyclones. Figure 6 shows a vertical cross section of temperature anomalies (temperature minus environmental temperature at each level) of Hurricane Bonnie on 25 August 1998 at 1230 UTC. The cross section is from 82° to 68°W with a vertical extent of approximately 50 000 ft (15.2 km). At this time the central location of Bonnie was near 29°N and 75°W. The cross section clearly shows the warm core of the hurricane centered at an elevation of about 35 000 ft (10.7 km). It is remarkably similar to cross sections determined from aircraft penetrations (Fig. 7), including the extension of the warm anomaly down into the lower troposphere inside the eye. The negative temperature anomalies at lower levels are caused by heavy precipitation contamination of the lower AMSU channels (4–6). This contamination provides useful information on the location and intensity of precipitation.

For the research presented here, retrievals for 61 time periods from Hurricanes Bonnie, Georges, and Mitch, and Typhoon Zeb were made, and the maximum temperature anomaly was calculated (Table 3).

b. Tropical cyclone intensity estimates

An application of the upper-level warm temperature anomalies is in assessing the intensity of tropical cyclones (maximum 1-min average wind speed at 10 m). Using data from previous microwave instruments, several investigators have examined the relationship between temperature anomalies and the surface wind speed and central pressure of tropical cyclones (e.g., Kidder et al. 1978, 1980; Velden and

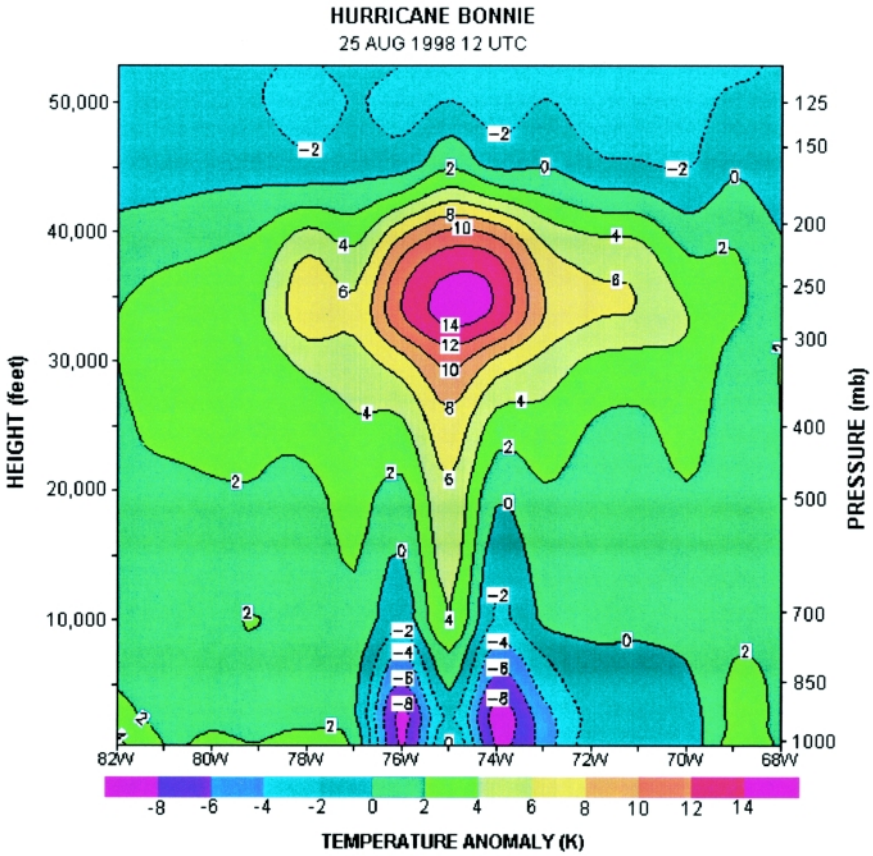

FIG. 6. Cross section of temperature anomalies through Hurricane Bonnie at 1200 UTC 25 Aug 1998 retrieved from AMSU data.

Smith 1983; Velden 1989; Velden et al. 1991). The much higher spatial resolution of the AMSU allows one to more accurately estimate the storm intensity. We related the maximum temperature anomaly near the center of the storm to surface wind speeds and central pressures obtained from operational track data. Figure 8 shows the results for four storms. In general, the temperature anomalies closely follow both the wind speeds and the pressures. Gaps in the data are caused by the storm being located between orbital swaths or by missing AMSU data.

Scatterplots of wind speed and central pressure versus AMSU temperature anomaly are shown in Fig. 9. Using only AMSU maximum temperature anomaly data, it appears that the surface wind speed can be estimated to within approximately 19 kt (10 m s^{-1}), and central pressure can be estimated within approximately 13 mb. Finally, grouping the AMSU maximum temperature anomalies by storm category gives an indication of how well the AMSU can categorize tropical cyclones (Fig. 10). Although the separation between categories is not large in this small sample of storms, the technique is simple to implement and appears promising for an analysis of storm category that complements the Dvorak techniques.

It can be seen in Fig. 9 that there is notable scatter in the data. One of the reasons for this is that the AMSU-A resolution of 48 km—though much better than previous microwave sounders—is still not small in comparison with the size of a tropical cyclone's central core or eye. Based on earlier work by Merrill (1995) using data from the MSU, this has two effects. First, the storm center may fall "between" sensor beam positions or footprints. Second, at the limb, the footprints become large (see Fig. 1), which compounds the first problem. As Merrill (1995) shows, the "bracketing effect" (storm eye falling in between adjacent half-power footprints) decreases the effective accuracy of the warm anomaly measurements. Work is under way (Velden and Brueske 1999) to develop a method to better estimate the warm anomaly from the AMSU raw radiance information. This algorithm attempts to address the above problems by explicitly modeling the interaction of the anomaly structure with the antenna gain patterns and scan geometry. The thermal anomaly is approximated by an analytic function whose parameters are estimated from a maximum-likelihood algorithm with constraints analogous to that used for thermodynamic soundings or optimal interpolation (Merrill 1995). The adjusted warm anomaly radiances will be used to reevaluate the statistical algorithms above for estimating tropical cyclone intensity.

c. *AMSU, AVHRR, and GOES imagery*

Because microwaves penetrate clouds, the AMSU provides views of the structure inside tropical cyclones that are not observable with visible and infrared sensors. The temperature anomalies discussed above are one such example. Another is the ability of window channels to sense precipitation-sized particles through the central dense overcast (CDO). Figure 11 shows

Hurricane Georges when it was officially a category 1 storm. The enhanced infrared image shows a well-developed CDO and outer bands. The 89-GHz image penetrates the CDO to show precipitation and an eye under the CDO. At 150 GHz, the eye is better depicted because enhanced sensitivity to precipitation causes greater contrast between the eye and eyewall.

It is always desirable to compare two or more observations of storms. Figure 12 shows three images of Hurricane Mitch: a composite AVHRR image, an AMSU image, and a GOES IR image. Flying with the AMSU on *NOAA-15* is the Advanced Very High Resolution Radiometer (AVHRR), which has a 1.1-km resolution in six visible and infrared channels. The extremely high resolution of the AVHRR infrared channels [~4 times higher than the more familiar Geostationary Operational Environmental Satellite (GOES) imager] makes comparison of visible, infrared, and microwave data attractive. Also, the much more frequent GOES images are an indispensable tool for monitoring hurricanes. The warm core of a tropical cyclone consists of two parts: a broad-scale, upper-level component, representing the overall magnitude of the tropical cyclone, and a small-scale, low-level warm core that is contained within the eye. Only occasionally (such as in Fig. 6) is the eye large enough and the satellite pass close enough to the center of the storm so that the lower-level temperature anomaly can be observed. The upper-level warming can always be observed, but the lower-level warming is often obscured by the surrounding rain or is simply smaller than the 48-km resolution of the AMSU-A instrument. It is necessary, therefore, to have an independent estimate of the size of the eye of a storm, which can be provided by GOES or AVHRR imagery.

d. Gradient wind retrieval

In the above sections it was shown that the AMSU temperature retrievals capture the warm anomalies associated with the tropical cyclones. If the AMSU temperature data were included in the three- and four-dimensional data assimilation systems employed at most numerical weather prediction centers, contributions to both the mass and wind fields of the analysis would result. Another method for obtaining wind information from the temperature fields is to assume a balance between the mass and wind fields. To gain some insight into the wind information contained within the AMSU temperature analyses, gradient and hydrostatic balance will be assumed. The procedure will be illustrated with the 1200 UTC data from

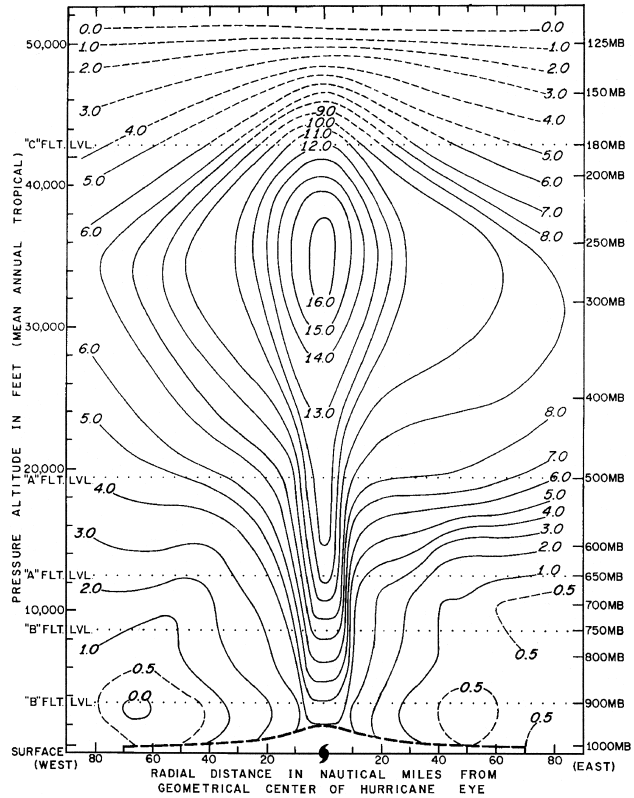

FIG. 7. Cross section of temperature anomalies through Hurricane Hilda (1964) [(after Hawkins and Rubsam (1968)].

Hurricane Bonnie on 25 August 1998, because the center of the AMSU data swath passed close to the center of the storm at this time, as shown in Fig. 13.

AMSU temperature soundings were retrieved at 40 vertical levels from 0.1 to 1000 mb at the grid locations shown in Fig. 13. Because the 1000-mb level could be below the surface near the center of the storm, the temperature data at this level were not used. Also, data above 50 mb were not used. The gradient wind calculation used the AMSU temperature data at 22 levels from 920 to 50 mb.

To determine the tangential winds from the gradient wind equation, it is necessary to calculate the pressure gradient. The first step is to determine the temperature as a function of radius and pressure. This was accomplished by interpolating the temperature data at each pressure level to a radial grid with the origin at the storm center (28.7°N, 74.7°W). The center position was obtained from the NHC best track. The spacing of the grid was 25 km, and the maximum radius was 500 km. The interpolation was performed using a simple scan analysis with a Gaussian weighting function. For example, the temperature T_i at radial grid point r_i is given by

TABLE 3. Storm data used in this study. Date and time style used is mm/dd/yy/UTC.

Storm	Date and time	Lat (°)	Long (°)	Wind speed (kt)	Central pressure (mb)	Category	Max. AMSU temp anomaly (K)
1 Bonnie	08/20/98/2100	17.90	–60.70	45	1004	Tropical storm	3.8
2 Bonnie	08/29/98/0000	37.80	–72.10	60	993	Tropical storm	4.5
3 Bonnie	08/20/98/1200	17.50	–55.50	30	1005	Tropical depression	5.1
4 Bonnie	08/21/98/1200	20.20	–64.60	45	1001	Tropical storm	7.2
5 Bonnie	08/28/98/1200	36.90	–74.50	65	990	Hurricane 1	7.3
6 Bonnie	08/22/98/1200	22.40	–70.00	70	984	Hurricane 1	8.8
7 Bonnie	08/25/98/0000	26.75	–73.00	100	963	Hurricane 3	9.1
8 Bonnie	08/27/98/1300	35.10	–77.00	65	975	Hurricane 1	9.3
9 Bonnie	08/24/98/1200	25.50	–72.50	100	963	Hurricane 3	10.2
10 Bonnie	08/26/98/1200	32.70	–77.80	100	965	Hurricane 3	11.0
11 Bonnie	08/23/98/1200	24.00	–71.70	90	959	Hurricane 2	11.1
12 Bonnie	08/26/98/0000	31.00	–76.50	100	958	Hurricane 3	12.6
13 Bonnie	08/25/98/1200	28.80	–74.30	100	963	Hurricane 3	13.4
14 Georges	09/24/98/0000	20.30	–75.30	65	992	Hurricane 1	4.1
15 Georges	09/25/98/0000	22.90	–79.00	75	987	Hurricane 1	5.8
16 Georges	09/27/98/0000	27.00	–86.50	95	970	Hurricane 2	5.9
17 Georges	09/16/98/0900	10.20	–30.30	30	1006	Tropical depression	6.1
18 Georges	09/18/98/0900	12.90	–45.20	80	978	Hurricane 1	6.5
19 Georges	09/24/98/1200	21.10	–77.00	65	989	Hurricane 1	6.7
20 Georges	09/17/98/2100	12.50	–41.10	65	987	Hurricane 1	7.0
21 Georges	09/20/98/2100	16.50	–59.90	115	956	Hurricane 4	7.5
22 Georges	09/23/98/1200	19.80	–73.80	65	987	Hurricane 1	7.5
23 Georges	09/29/98/1200	31.00	–88.00	35	993	Tropical storm	8.1
24 Georges	09/26/98/0000	24.70	–83.10	90	974	Hurricane 2	8.3
25 Georges	09/26/98/1200	25.80	–85.05	90	974	Hurricane 2	8.6
26 Georges	09/29/98/0000	30.70	–89.00	45	977	Tropical storm	9.1
27 Georges	09/21/98/1200	17.50	–63.70	95	966	Hurricane 2	9.8
28 Georges	09/22/98/0100	18.20	–66.40	100	975	Hurricane 3	9.9
29 Georges	09/22/98/1100	18.20	–68.30	95	970	Hurricane 2	10.5

TABLE 3. *(Continued.)*

30 Georges	09/25/98/1300	24.20	–81.50	85	982	Hurricane 2	10.6
31 Georges	09/28/98/0100	29.30	–88.50	95	961	Hurricane 2	11.4
32 Georges	09/27/98/1500	28.40	–88.00	95	963	Hurricane 2	11.5
33 Georges	09/20/98/0000	15.80	–55.00	130	938	Hurricane 4	11.6
34 Georges	09/28/98/1300	30.40	–89.00	85	965	Hurricane 2	13.9
35 Georges	09/20/98/1200	16.10	–57.80	130	939	Hurricane 4	14.3
36 Mitch	11/01/98/0300	14.60	–90.50	30	1002	Tropical depression	4.5
37 Mitch	11/01/98/1200	14.95	–91.50	28	1004	Tropical depression	4.8
38 Mitch	10/22/98/0300	12.80	–77.90	30	1001	Tropical depression	5.5
39 Mitch	10/30/98/1200	15.40	–86.10	35	997	Tropical storm	5.8
40 Mitch	11/04/98/0000	20.00	–90.60	40	997	Tropical storm	5.8
41 Mitch	10/23/98/0100	11.90	–77.60	43	1000	Tropical storm	6.0
42 Mitch	10/22/98/1500	12.00	–78.00	30	1001	Tropical depression	6.3
43 Mitch	10/29/98/1500	16.00	–85.60	65	987	Hurricane 1	6.7
44 Mitch	10/29/98/0000	16.30	–86.00	90	966	Hurricane 2	7.0
45 Mitch	10/30/98/0000	15.50	–85.80	50	995	Tropical storm	7.1
46 Mitch	10/28/98/1200	16.40	–85.60	105	949	Hurricane 3	8.7
47 Mitch	10/26/98/0000	16.50	–81.40	130	924	Hurricane 4	13.0
48 Mitch	10/26/98/1200	16.60	–82.60	135	923	Hurricane 5	14.5
49 Mitch	10/27/98/0000	17.30	–83.80	155	906	Hurricane 5	15.0
50 Mitch	10/27/98/1200	17.40	–85.20	155	917	Hurricane 5	19.0
51 Zeb	10/10/98/1000	10.80	139.43	33	—	Tropical depression	5.8
52 Zeb	10/10/98/2200	10.30	137.60	47	—	Tropical storm	6.6
53 Zeb	10/16/98/1200	26.50	124.60	80	—	Typhoon 1	6.6
54 Zeb	10/11/98/0900	10.70	135.40	53	—	Tropical storm	7.2
55 Zeb	10/11/98/2200	10.93	132.90	70	—	Typhoon 1	9.2
56 Zeb	10/14/98/1000	17.63	121.53	105	—	Typhoon 3	9.4
57 Zeb	10/15/98/1200	121.50	121.20	80	—	Typhoon 1	9.4
58 Zeb	10/12/98/1200	12.80	129.90	90	—	Typhoon 2	10.2
59 Zeb	10/15/98/0000	19.10	120.50	85	—	Typhoon 2	12.2
60 Zeb	10/13/98/1000	15.87	125.07	153	—	Typhoon 5	18.3
61 Zeb	10/14/98/0000	17.10	122.50	155	—	Typhoon 5	19.8

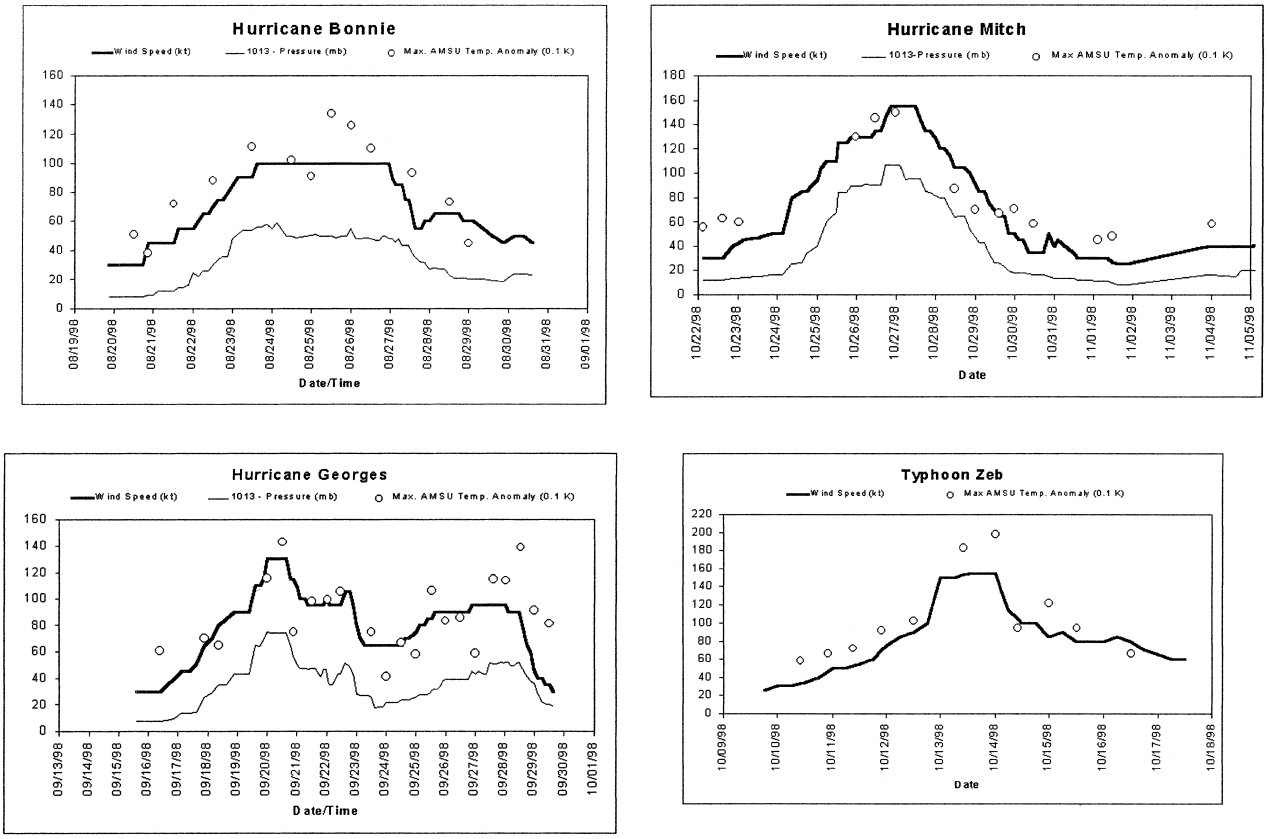

FIG. 8. Plots of wind speed, central pressure, and maximum temperature anomaly (retrieved from AMSU data) as functions of time for Hurricanes Bonnie, Georges, and Mitch, and Typhoon Zeb. (Central pressures were not available for Zeb.)

$$T_i = \Sigma w_k T_k / \Sigma w_k, \tag{4.1}$$

where the summations in (4.1) are over all of the observations T_k at a given pressure level and the weights w_k are given by

$$w_k = \exp[-(r_i - r_k)^2 / r_e^2]. \tag{4.2}$$

The parameter r_e determines the smoothness of the interpolated field and was set to 30 km. This choice is consistent with the maximum resolution of the data in Fig. 13, which is about 50 km.

AMSU soundings do not provide an estimate of the surface temperature or pressure. A constant surface temperature—equal to the sea surface temperature (SST) near the storm center minus 1 K—was assumed. Although Cione et al. (1999) have shown that this assumption may not be valid near the storm center, the retrieved pressures and winds are not very sensitive to variations of 1–2 K in the assumed surface temperature. The SST for this case was 28.2°C as determined from the National Centers for Environmental Prediction (NCEP) weekly SST analyses. The surface pressure at the outer radius of the radial grid (1012 mb) was estimated from the initial analysis for the NCEP global forecast model. Once the surface pressure and temperature were estimated at the outer radius, the hydrostatic equation was integrated upward to determine the height of the first AMSU pressure level (920 mb). For the integration, it was assumed that the temperature varied linearly with height in the layer. In addition, the effect of moisture (the virtual temperature correction) was neglected in the hydrostatic calculation due to the lack of water vapor observations near the storm center. The errors associated with this approximation should be much less than the errors in the mass field due to the limited horizontal resolution of the data. This procedure was repeated in each layer to give the height of each pressure level up to 50 mb at the outer radius.

Next, it was assumed that 50 mb was above the storm circulation, so that the height of this level was constant with radius all the way to the storm center. Given the height of the 50-mb level, the hydrostatic equation was then integrated downward at all radii (except the outer radius) to give the height at each pressure level down to 920 mb. Then, given the height and

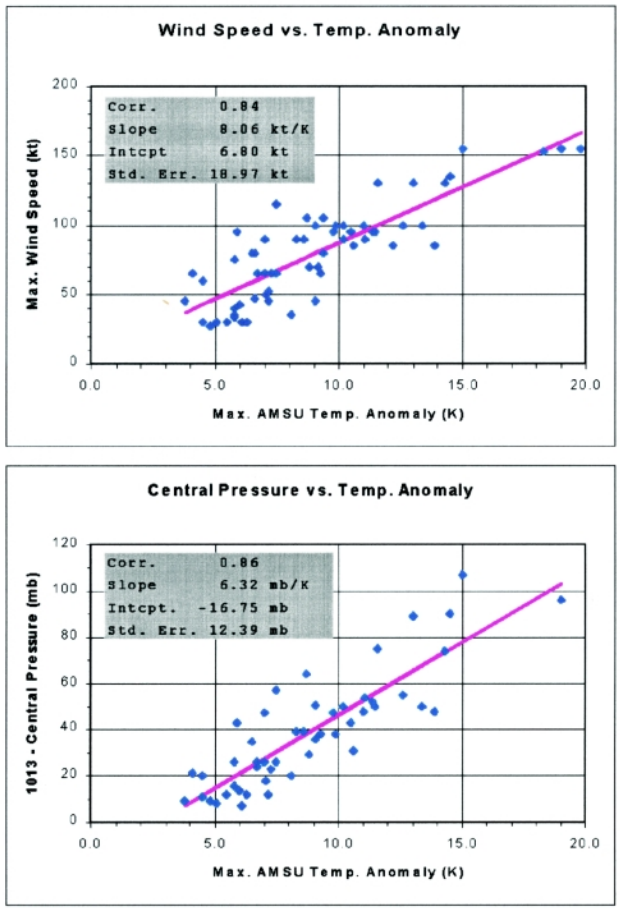

FIG. 9. Scatterplots of central pressure and intensity versus maximum retrieved AMSU temperature anomaly for Hurricanes Bonnie, Georges, and Mitch, and Typhoon Zeb.

temperature of the 920-mb level and the assumed surface temperature, the hydrostatic equation was used to calculate the surface pressure.

Once the above calculations were complete, the surface temperature and pressure, and the temperature and height at each pressure level from 920 to 50 mb were known. With the assumption of a linear variation of temperature with height between the pressure levels, it is then possible to calculate the pressure and temperature at any height. These variables were calculated at 1-km intervals from the surface to 20 km. Given the temperature and pressure at the height levels, the density was determined from the ideal gas equation.

The final step was to calculate the pressure gradient in the gradient wind equation using centered derivatives for the radial derivative of pressure, with a one-side difference at the outer radius. Given the pressure gradient, the tangential wind was calculated as a function of radius and height, where the Coriolis parameter was evaluated at the latitude of the storm center. When the radial pressure gradient is negative and its magnitude exceeds $f^2r/4$ (where f is the Coriolis parameter) there is no real solution for the tangential wind. This problem occurred at a few radii in the upper levels. In these cases, the magnitude of the pressure gradient was reduced to the largest value for which there was a real solution.

Figure 14 shows the perturbation temperature as a function of radius and height, where the perturbation was calculated by subtracting the temperature at the maximum radius from the temperature at each radius. This figure shows that there is a maximum warm anomaly near 11 km, with cold anomalies above 16 km and in the lowest few kilometers. As described previously, the low-level cold anomalies are due to attenuation by heavy precipitation and may not be representative of the actual thermal structure.

Figure 15 shows the tangential wind as a function of radius and height. The basic structure of the storm seems reasonable, with low-level cyclonic flow and an upper-level anticyclone. The maximum low-level tangential wind is 42 m s^{-1} at a radius of about 100 km. The radius of maximum wind slopes outward with height, which is typical of intense tropical cyclones. The radius of maximum wind is somewhat large for a storm of hurricane strength. However, as will be shown below, Bonnie was a fairly large storm, and the radius of maximum wind is similar to that observed by U.S. Air Force Reserve reconnaissance aircraft.

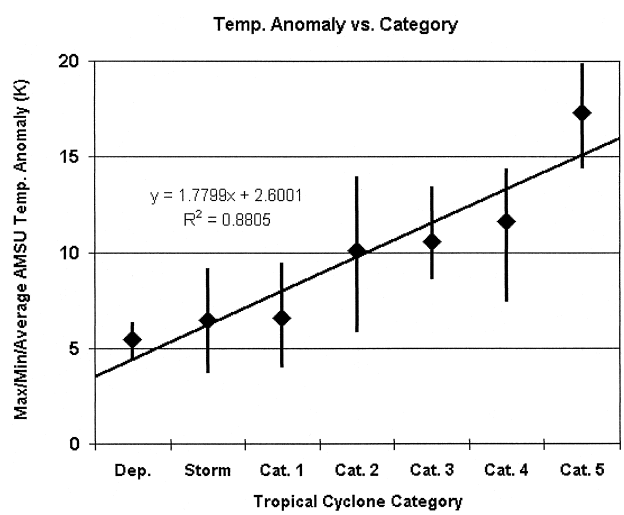

FIG. 10. Maximum AMSU temperature anomaly (K) vs tropical cyclone category. The diamond symbol indicates the mean temperature anomaly in that category. The vertical line extends from the largest to the smallest temperature anomaly in that category. The regression line indicates that for each 1.8-K rise in the AMSU temperature anomaly, the storm advances one category.

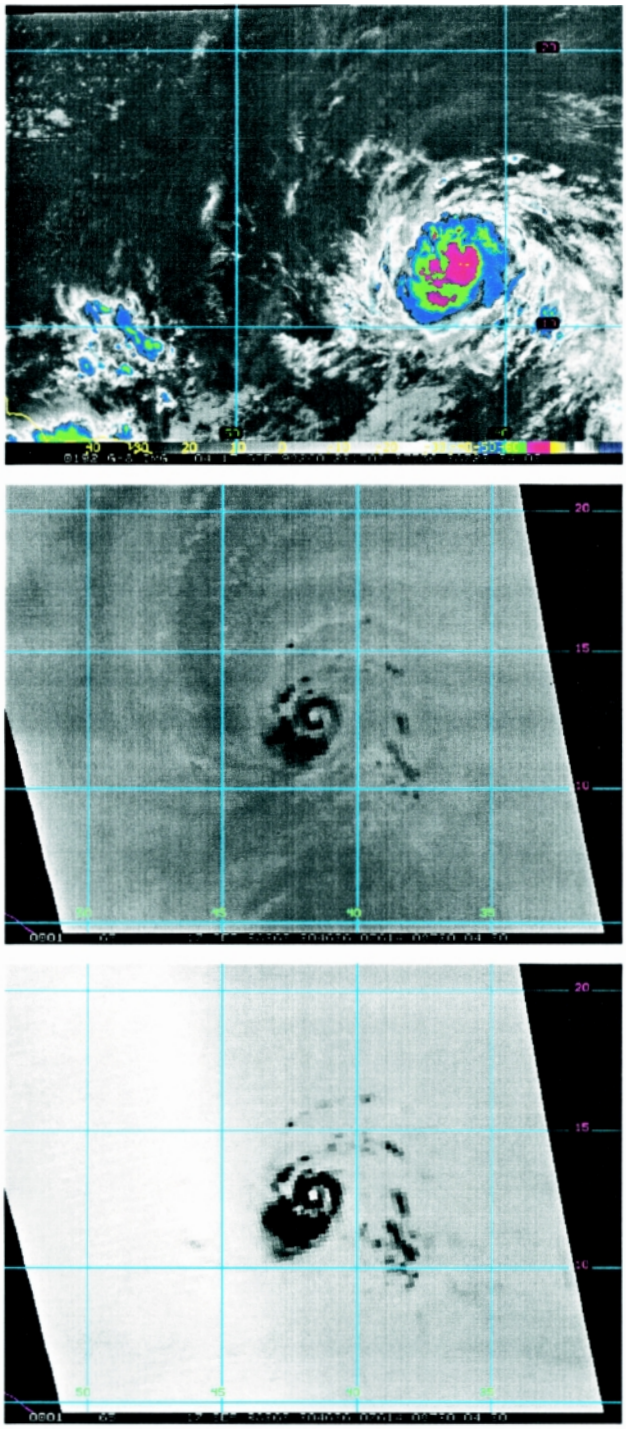

FIG. 11. Hurricane Georges near 2215 UTC 17 Sep 1998. (top) Enhanced infrared image showing the central dense overcast and outer banding. (middle) AMSU-B 89-GHz image showing a definite eye (light spot at center) and banding under the CDO. (bottom) AMSU-B 150-GHz image, which better depicts the eye because of enhanced sensitivity due to scattering in the eyewall and rainbands. This image also shows the effects of the radio frequency interference (brightening on the left side of the image), which has caused problems for AMSU-B. A solution for this problem is being pursued.

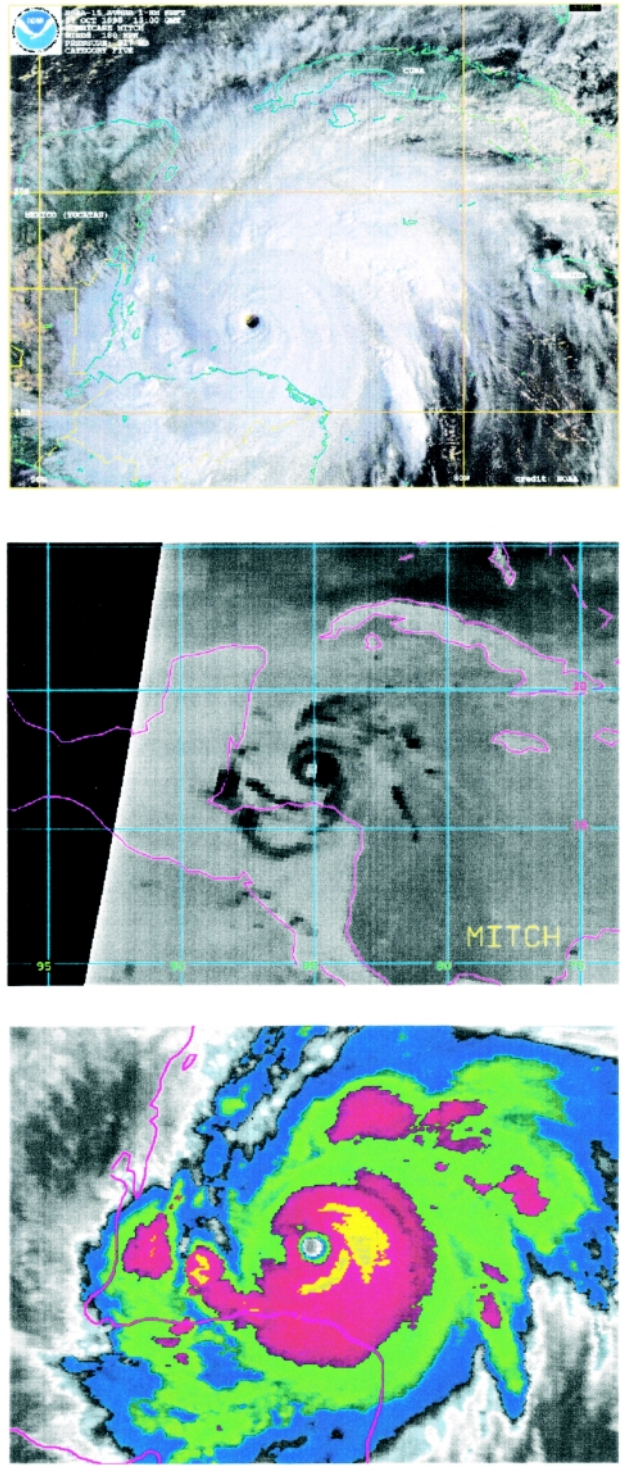

FIG. 12. (top) Composite AVHRR image of Hurricane Mitch constructed from 1.1-km resolution data. (middle) AMSU-B 89-GHz image of Hurricane Mitch at exactly the same time as the AVHRR image above, constructed from 16-km resolution data and presented at 4-km resolution. (bottom) *GOES-10* infrared image of Hurricane Mitch within minutes of the time of the images above, constructed from 4-km resolution data and presented at 2-km resolution.

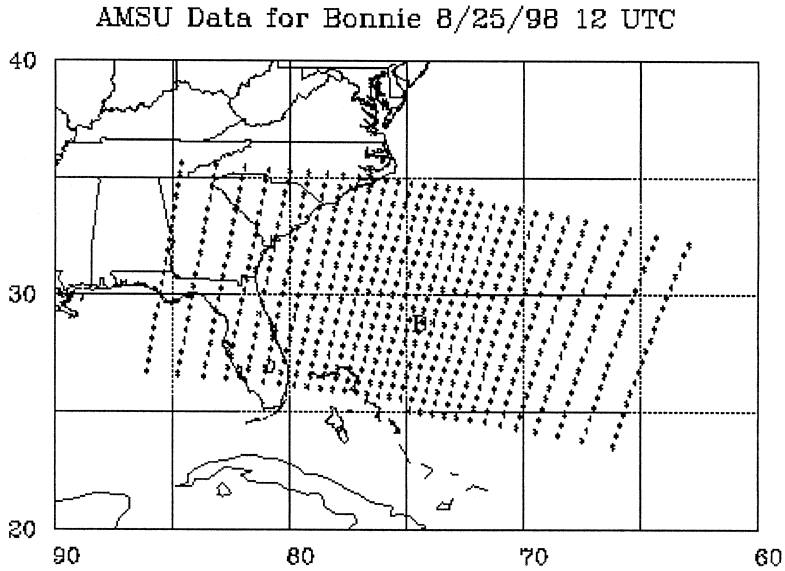

FIG. 13. Locations of the AMSU temperature data used in the gradient wind retrieval for Hurricane Bonnie at 1200 UTC 25 Aug 1998. The storm center is indicated by the uppercase B.

According to the NHC best track, the maximum winds were 52 m s^{-1} (100 kt) at this time. However, the NHC maximum winds could be at a single point, while the gradient wind is an azimuthal average. Thus, it should be expected that the gradient wind would be less than the maximum wind. On the other hand, the gradient wind calculation does not include frictional effects and is probably more representative of the winds at the top of the boundary layer. Thus, it appears that the gradient wind retrieval underestimated the storm maximum wind. As described above, the surface pressure is also calculated as part of the gradient wind procedure. The minimum surface pressure (at $r = 0$) from the retrieval was 978 mb, compared to a minimum pressure from the NHC best track of 966 mb. These values are consistent with an underestimate of the storm intensity. It is likely that the resolution of the AMSU data and the attenuation by the liquid water led to the underestimates. However, the data still provide information about the general storm structure that is not available by any other means.

Although the general structure near the storm center appears reasonable near the radius of maximum wind, the outer wind structure looks less realistic in Fig. 15. For example, the flow becomes anticyclonic in the low levels for radii greater than about 300 km. This structure is probably due to the unrealistic cold (precipitation) anomalies below 6 km.

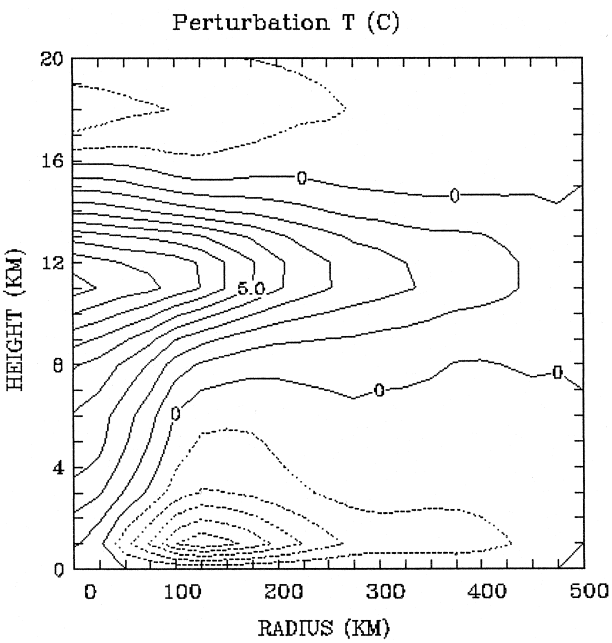

FIG. 14. The azimuthally averaged perturbation temerature as a function of radius and height for Hurricane Bonnie at 1200 UTC 25 Aug 1998. The contour interval is 1 K.

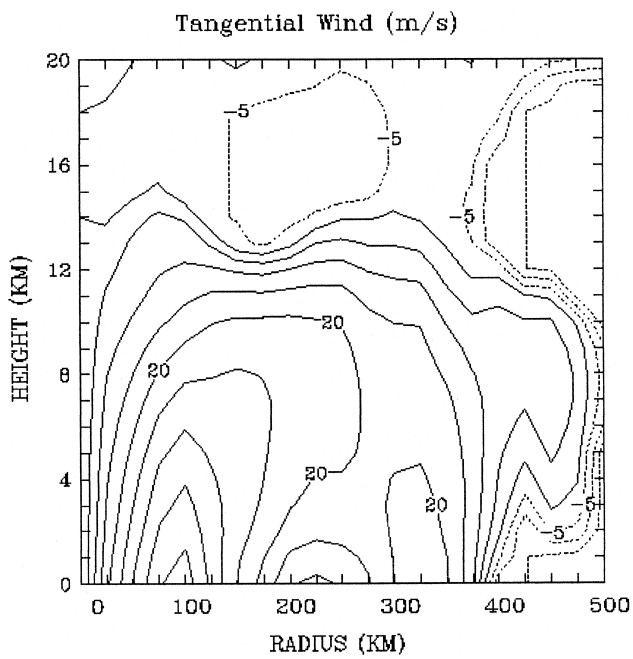

FIG. 15. The azimuthally averaged tangential wind as a function of radius and height for Hurricane Bonnie at 1200 UTC 25 Aug 1998. The contour interval is 5 m s^{-1}. Negative values indicate anticyclonic flow.

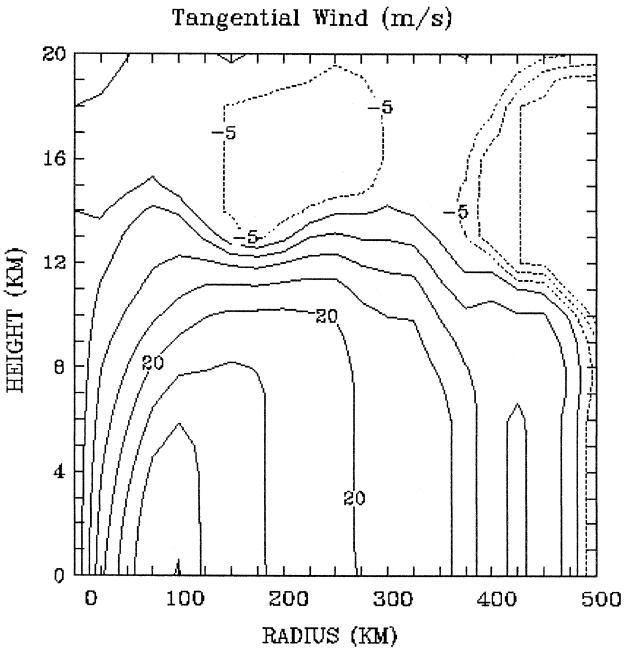

FIG. 16. Same as Fig. 15 except after the low-level cold anomalies have been removed.

To reduce the effect of the low-level cold anomalies, the temperature anomalies at pressure levels between the surface and 500 mb were set to zero and the gradient winds were recalculated. Figure 16 shows the tangential winds after this adjustment. The tangential wind at large radius appears more reasonable, suggesting that methods should be developed to address the precipitation attenuation problem.

Quantitative validation of the entire wind field in Fig. 15 or Fig. 16 is a difficult task due to the lack of other observations. However, the U.S. Air Force Reserve flew a reconnaissance mission close to the time of the AMSU pass. A "figure 4" pattern with radial legs extending out to a little beyond 200 km was flown at the 3-km level. The wind observations from this flight within 6 h of the AMSU pass were put into a storm-relative cylindrical coordinate system and then analyzed using the variational procedure described by DeMaria et al. (1999). Figure 17 shows the azimuthally averaged tangential wind from the aircraft data (out to 250 km) and the tangential wind at 3 km from the AMSU gradient wind retrieval for the case with and without the low-level temperature adjustment. The aircraft data show that the radius of maximum wind was quite large (about 100 km), consistent with the AMSU gradient winds. The average difference between the aircraft and AMSU winds (out to 250 km) was 4.6 and 4.4 m s^{-1} for the adjusted and unadjusted cases, respectively. The AMSU winds show a secondary wind maximum near 350 km. Unfortunately, the aircraft did not fly far enough from the storm center to verify this feature. These results again show the potential to obtain valuable wind information from the AMSU temperature retrievals. Further study is necessary to evaluate the utility and limitations of the data, especially in cases with smaller radii of maximum winds.

e. Estimation of tropical cyclone precipitation potential

Since 1992, the Satellite Analysis Branch (SAB) of the National Environmental Satellite, Data and Information Service (NESDIS) has experimentally used the operational SSM/I rain rate product to produce a rainfall potential for tropical disturbances expected to make landfall within the next 24 h. The launch in 1998 of the first AMSU now provides us with an additional way to calculate rainfall potential from tropical disturbances worldwide. (The technique has not yet been applied to TRMM data.)

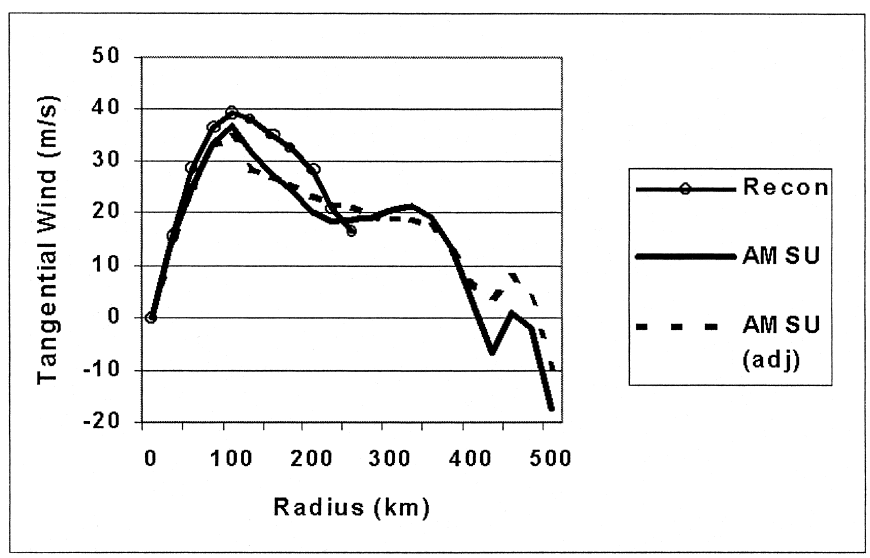

FIG. 17. The azimuthally averaged tangential wind at 3 km from the U.S. Air Force Reserve flight-level data and the AMSU gradient wind retrievals. The dashed line shows the AMSU winds after the low-level cold anomalies were removed. No aircraft data were available for radii greater than 250 km.

The experimental rainfall potential can use the operational SSM/I 14 km × 16 km (Ferraro et al. 1998) or the AMSU 48-km resolution objective rain rates (Grody et al. 1999) to produce an areal extent of rain and average rain rate through the storm in its direction of motion. In either case, the speed of the tropical disturbance and any modification of the rainfall potential based on the latest geostationary satellite imagery trends are incorporated into the calculations and results in the final Tropical Rainfall Potential (TRaP). Below is a description of how the technique was performed using the AMSU 48-km resolution rain rate product (Grody et al. 1999) for the case of Hurricane Georges as it was heading for the keys of south Florida.

In determining the TRaP for a tropical disturbance, the analyst applies a rainfall potential formula,

$$\mathrm{TRaP} = R_{\mathrm{av}} D V^{-1}, \qquad (4.3)$$

that is simplified from the NESDIS Operational Rainfall Estimation Technique (Spayd and Scofield 1984). Here, R_{av} is the average rain rate along a line in the direction of motion of the cyclone, D is the distance of that line across the rain area of the storm, and V is the actual speed of the tropical cyclone that can be measured using consecutive satellite images 3–6 h apart. If significant changes in the intensity or speed are noted between the time of the microwave pass and the time the TRaP is produced, an adjustment of the TRaP can be made based on the latest half-hourly geostationary satellite trends.

In the case of the 0023 UTC 25 September 1998 *NOAA-15* pass over Hurricane Georges, the SAB analyst drew a line A through the digital rain rate image (Fig. 18) in the direction of motion of the storm. Each digital rain rate in Fig. 18 represents the average microwave rain rate over a 48 km × 48 km area. It should be noted here, that in the future, a 16 km × 16 km rain rate area (similar to SSM/I) will be derived from AMSU-B measurements and should make the rainfall potential calculation more accurate. Line A resulted in an average rain rate (R_{av}) of 0.224 in. h^{-1} (5.69 mm h^{-1}), the distance (D) of the line was 6.0° latitude (667 km), and the speed (V) of the storm was 12 kt (22.2 km h^{-1}). A TRaP was calculated using the above formula and resulted in a maximum rainfall potential of 6.72 in. (170.6 mm). The observed rainfall in Key West was 8.38 in. (213 mm). This indicates that the AMSU rain rates might be a little low, but using them, one would have been able to forecast substantial rain in the Florida Keys.

f. Challenges

Although AMSU data are quite useful for tropical cyclone analysis, there are a few challenges. First, since AMSU is mounted on a polar orbiting satellite, it can view a tropical cyclone only twice per day. Significant changes in the storm can take place between observations. Second, AMSU observations are not contiguous at the equator; sometimes storms can "fall in the crack" (Fig. 19).

The above two challenges could be alleviated in a number of ways. If future microwave instruments were to scan a little farther toward the limb, the "gap" would be smaller. When more satellites carrying AMSU instruments are launched, the observation frequency will increase. Finally, a microwave instrument could be placed in geostationary orbit. This would solve both the temporal resolution problem and the gap problem; however, it presents a technical challenge because a

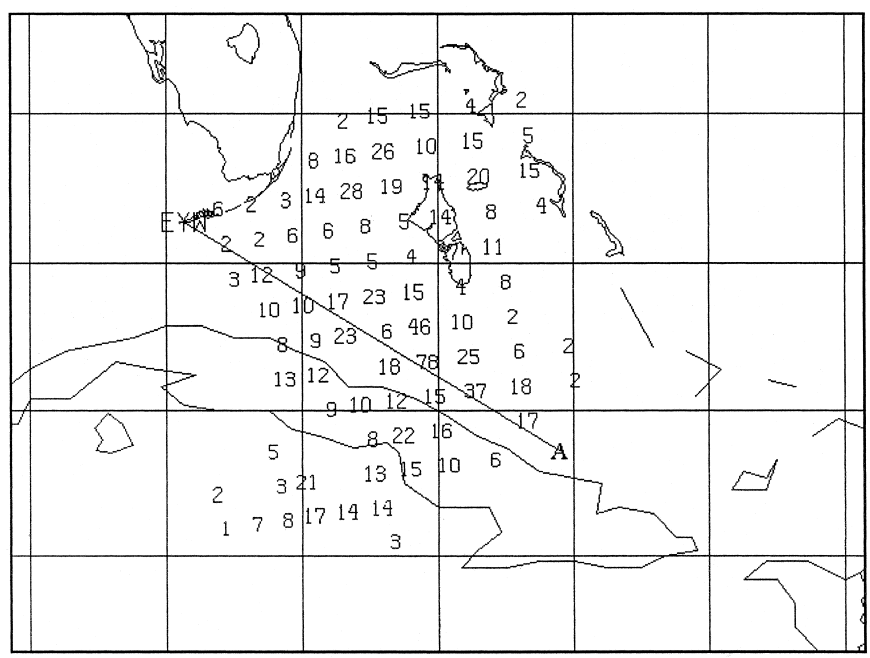

FIG. 18. Rain rates (0.01 in h^{-1}) in Hurricane Georges. The TRaP was calculated along line A.

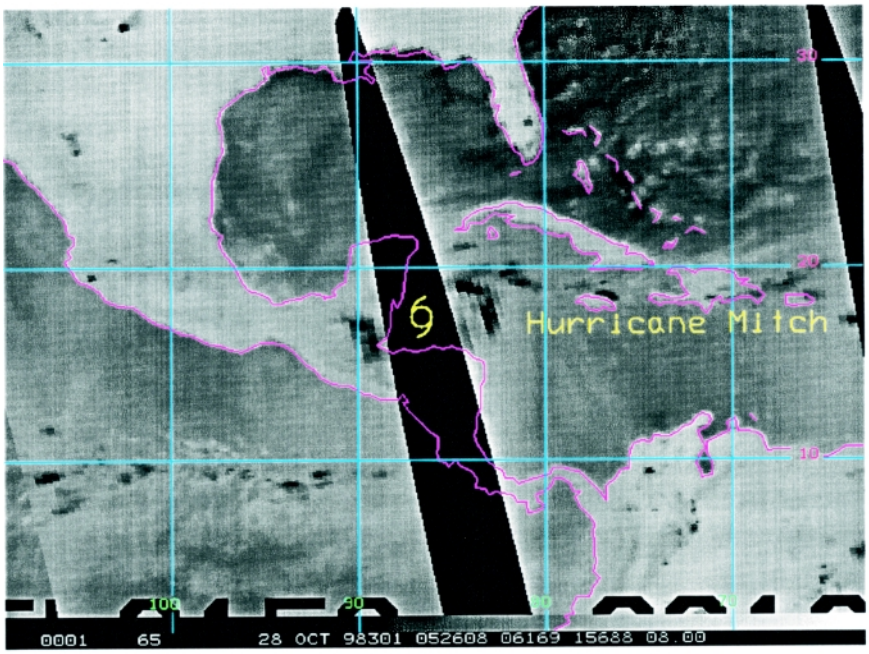

FIG. 19. An example of a tropical cyclone "falling in the crack" between AMSU swaths.

large antenna is required to make measurements with acceptable ground resolution. We encourage further study of a geostationary microwave instrument.

5. Summary and conclusions

The Advanced Microwave Sounding Unit flying on the *NOAA-15* satellite is the first of a series of microwave imager/sounders that can sense atmospheric temperature, moisture, and precipitation through clouds. In this paper, we have examined how the AMSU data can be applied to tropical cyclone analysis and forecasting. We presented 1) upper-tropospheric thermal anomalies in tropical cyclones retrieved from AMSU data, 2) the correlation of maximum temperature anomalies with maximum wind speed and central pressure, 3) winds calculated from the temperature anomaly field, 4) comparison of AMSU data with GOES and AVHRR imagery, and 5) tropical cyclone rainfall potential. Several conclusions can be drawn from this work.

- The results of four AMSU case studies suggest that the development of a new operational satellite-based algorithm for assigning tropical cyclone intensity is warranted. This product would use AMSU upper warm core measurements as a refinement to the Dvorak approach. A large representative sample with good validation data (from surface and aircraft observations) is needed for development and testing of an algorithm of this type.
- An estimate of the three-dimensional structure of the temperature, pressure, and wind fields can be derived from soundings retrieved from AMSU data. These promise to be quite useful in monitoring the storms, in issuing watches and warnings, and perhaps in numerical model initialization.
- Precipitation potential for tropical cyclones can be calculated from the AMSU data and appears to be useful in forecasting the heavy precipitation associated with a landfalling tropical cyclone. More study is needed to determine the accuracy of the technique when performed using AMSU rain rates.

Though much more work remains to be done before the techniques presented here are finalized, we believe that the AMSU is extremely promising for improving our knowledge of tropical cyclones.

Acknowledgments. The support of the National Oceanic and Atmospheric Administration through NOAA Contract NA67RJ0152 is gratefully acknowledged by the first author. Acknowledgment is also given to Ralph Ferraro and Fuzong Weng of the NOAA/NESDIS/Microwave Sensing Group for helpful discussions. We also acknowledge the excellent work of Ms. Lihang Zhou for the development of the software to derive vertical cross sections of AMSU-A temperature retrievals in near–real time.

References

Adler, R. F., and E. B. Rodgers, 1977: Satellite-observed latent heat release in tropical cyclone. *Mon. Wea. Rev.,* **105,** 956–963.

Allison, L. J., 1974: Tropical cyclone rainfall as measured by the Nimbus 5 electrically scanning microwave radiometer. *Bull. Amer. Meteor. Soc.,* **55,** 1074–1089.

Cione, J. J., P. G. Black, and S. H. Houston, 1999: Cooling and drying within the hurricane near-surface environment. Preprints, *23d Conf. on Hurricanes and Tropical Meteorology,* Dallas, TX, Amer. Meteor. Soc., 1027–1030.

DeMaria, M., 1996: A history of hurricane forecasting for the Atlantic basin, 1920–1995. *Historical Essays on Meteorology 1919–1995,* J. R. Fleming, Ed., Amer. Meteor. Soc., 263–306.

——, F. M. Horsfall, and E. N. Rappaport, 1999: Incorporation ofaircraft observations in a Statistical Hurricane Intensity Prediction Scheme. Preprints, *23d Conf. on Hurricanes and Tropical Meteorology,* Dallas, TX, Amer. Meteor. Soc., 596–599.

Dvorak, V. F., 1973: A technique for the analysis and forecasting of tropical cyclone intensities from satellite pictures. NOAA Tech. Memo. NESS 45, Washington, DC, 19 pp.

——, 1975: Tropical cyclone intensity analysis and forecasting from satellite imagery. *Mon. Wea. Rev.,* **103,** 420–430.

——, 1984: Tropical cyclone intensity analysis using satellite data. NOAA Tech. Rep. NESDIS 11, Washington, DC, 47 pp.

Ferraro, R. R., S. J. Kusselson, and M. C. Colton, 1998: An introduction to passive microwave remote sensing and its applications. *Natl. Wea. Dig.,* **22,** 11–23.

Goldberg, M. D., 1999: Generation of retrieval products from AMSU-A: Methodology and validation. *10th Int. ATOVS Study Conf.,* Boulder, CO, 219–229.

Grody, N. C., 1979: Typhoon "June" winds estimated from scanning microwave spectrometer measurements at 55.45 GHz. *J. Geophys. Res.,* **84,** 3689–3695.

——, 1991: Classification of snowcover and precipitation using the special sensor microwave imager. *J. Geophys. Res.,* **96,** 7423–7435.

——, and W. C. Shen, 1982: Observation of Hurricane David (1979) using the Microwave Sounding Unit. NOAA Tech. Rep. NESS 88, Washington, DC, 52 pp.

——, F. Weng, and R. Ferraro, 1999: Application of AMSU for obtaining water vapor, cloud liquid water, precipitation, snow cover, and sea ice concentration. *10th Int. ATOVS Study Conf.,* Boulder, CO, 230–240.

Hawkins, H. F., and D. T. Rubsam, 1968: Hurricane Hilda, 1964 II. Structure and budgets of the hurricane on October 1, 1964. *Mon. Wea. Rev.,* **96,** 617–636.

Kidder, S. Q., and T. H. Vonder Haar, 1995: *Satellite Meteorology: An Introduction.* Academic Press, 466 pp.

——, W. M. Gray, and T. H. Vonder Haar, 1978: Estimating tropical cyclone central pressure and outer winds from satellite microwave data. *Mon. Wea. Rev.,* **106,** 1458–1464.

——, ——, and ——, 1980: Tropical cyclone outer surface winds derived from satellite microwave data. *Mon. Wea. Rev.,* **108,** 144–152.

Kummerow, C., W. Barnes, T. Kozu, J. Shiue, and J. Simpson, 1998: The Tropical Rainfall Measuring Mission (TRMM) sensor package. *J. Atmos. Oceanic. Technol.,* **15,** 809–817.

Merrill, R. T., 1995: Simulations of physical retrieval of TC thermal structure using 55-GHz band passive microwave observations from polar-orbiting satellites. *J. Appl. Meteor.,* **34,** 773–787.

Mo, T., 1999: AMSU-A antenna pattern corrections. *IEEE Trans. Geosci. Remote Sens.,* **37,** 103–112.

Purdom, J. F. W., and W. P. Menzel, 1996: Evolution of satellite observations in the United States and their use in meteorology. *Historical Essays on Meteorology 1919–1995,* J. Fleming, Eds., Amer. Meteor. Soc., 99–156.

Rodgers, E. B., and R. F. Adler, 1981: Tropical cyclone rainfall characteristics as determined from a satellite passive microwave radiometer. *Mon. Wea. Rev.,* **109**, 506–521.

Rosenkranz, P. W., D. H. Staelin, and N. C. Grody, 1978: Typhoon June (1975) viewed by a scanning microwave spectrometer. *J. Geophys. Res.,* **83,** 1857–1868.

Sheets, R. C., 1990: The National Hurricane Center—Past, present, and future. *Wea. Forecasting,* **5,** 185–232.

Spayd, L. E., Jr., and R. A. Scofield, 1984: A tropical cyclone precipitation estimation technique using geostationary satellite data. NOAA Tech. Memo. NESDIS 5, 36 pp.

Spencer, R. W., 1993: Global oceanic precipitation from the MSU during 1979–91 and comparisons to other climatologies. *J. Climate,* **6,** 1301–1326.

Velden, C. S., 1989: Observational analyses of North Atlantic tropical cyclones from NOAA polar-orbiting satellite microwave data. *J. Appl. Meteor.,* **28,** 59–70.

——, and W. L. Smith, 1983: Monitoring tropical cyclone evolution with NOAA satellite microwave observations. *J. Climate Appl. Meteor.,* **22,** 714–724.

——, and K. F. Brueske, 1999: Tropical cyclone warm cores as observed from the NOAA polar orbiting satellite's new Advanced Microwave Sounding Unit. Preprints, *23d Conf. on Hurricanes and Tropical Meteorology,* Dallas, TX, Amer. Meteor. Soc., 182–185.

——, B. M. Goodman, and R. T. Merrill, 1991: Western North Pacific tropical cyclone intensity estimation from NOAA polar-orbitingsatellite microwave data. *Mon. Wea. Rev.,* **119,** 159–168.

——, T. L. Olander, and R. M. Zehr, 1998: Development of an objective scheme to estimate tropical cyclone intensity from digital geostationary satellite infrared imagery. *Wea. Forecasting,* **13,** 172–186.

Wark, D. Q., 1993: Adjustment of TIROS Operational Vertical Sounder data to a vertical view. NOAA Tech. Rep. NESDIS 64, Washington, DC, 36 pp.

Weng, F., and N. Grody, 1994: Retrieval of cloud liquid water using the Special Sensor Microwave Imager (SSM/I). *J. Geophys. Res.,* **99,** 25 535–25 551.